Probing the electronic states of band ferromagnets with photoemission

Thomas Greber

Physik Institut der Universität Zürich, Switzerland

Haeraeus-Seminar "Ground-State and Finite-Temperature Bandferromagnetism"
Berlin Wandlitz, October 4-6 2000, (Version April 10, 2001)

Abstract. Angle scanned photoemission experiments that map the electronic band structure up to $5k_BT$ above the Fermi level are reviewed. After a short tutorial of the basic principles for the interpretation of angular resolved photoemission (ARUPS) experimental data on the band ferromagnet nickel are presented. The exchange splitting of the *sp*–bands and the *d*–bands can be accurately determined. The influence of the temperature and adsorbate layers on the magnetism of the surface are investigated.

For clean nickel metal the ferromagnetic – paramagnetic phase transition is observed in detail. It is found that the exchange splitting follows - within the accuracy of the experiment - the bulk magnetization and disappears at the Curie temperature [1]. A magnetically "active" region in **k**-space, where *sp* and *d* minority bands coincide on the Fermi surface is inspected.

A monolayer of hexagonal boron nitride on Ni(111) strongly influences the Fermi surface of the interface. The formally insulating *h*-BN acts as an atomic grating and induces umklapp processes. It is seen how the exchange splitting is affected and that the overlayer changes the relative spin asymmetry of exchange split *sp*-bands.

1 Introduction

Photoemission is among the few techniques that gives experimental access to all relevant electronic states at surfaces that constitute e.g. band ferromagnetism, superconductivity or chemical bonding. For the case of band ferromagnets this was realized with the early experiments of Pierce and Spicer [2] who observed the ferro- paramagnetic phase transition in nickel and in the same issue of Bänninger et al. who measured below the Curie temperature spin polarized photoelectrons from nickel [3]. In the mean time the technique of photoemission has matured close to the complete photoemission experiment where all degrees of freedom of the photoelectrons are measured in the same setup.

For the study of phase transitions in metals it is generally accepted that the states at the Fermi level are the key players. All electronic states around the Fermi level should be accessed in order to get a complete picture.

Photoemission is very fast and localized. It suffers, however, from the $N \rightarrow N-1$ "problem" i.e. the interaction of the hole state that is created in the photoemission process. Its influence on the photoelectron may not be neglected – in particular in correlated systems like a band ferromagnet and makes comparisons with ground state calculations challenging.

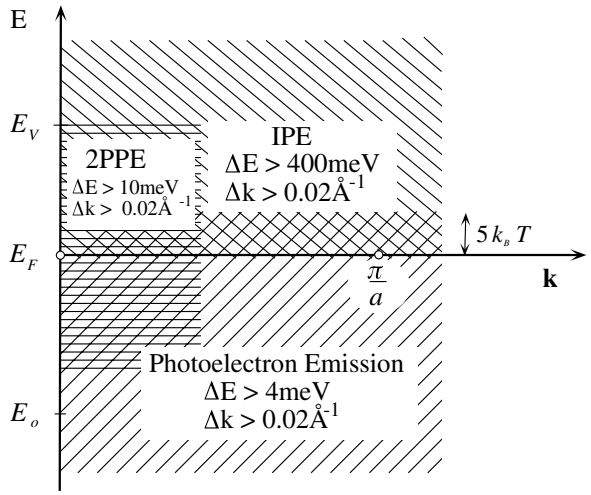

Fig. 1. Accessible energies and k-space for different experimental methods. The energy-resolution ΔE and k-resolution Δk are given for Two Photon Photoelectron Emission (2PPE), Inverse Photoemission (IPE) and photoelectron emission. The relevant energies, the Fermi energy E_F, band bottom E_o and vacuum energy E_V are indicated as well as the Brillouin zone boundary π/a.

2 Experimental

In Fig.1 the electron energies and k-vectors that can be measured with k-resolving techniques like Inverse PhotoEmission (IPE), Two Photon Photo-Emission (2PPE) and PhotoEmission (PE) are shown. 2PPE, as it is performed today, has - like Scanning Tunneling Spectroscopy (STS) - the potential of probing the occupied and unoccupied electronic states. It suffers, however, from the relatively low energies and k-vectors that can be reached and is thus unable to probe the whole Brillouin zone. This is not the case in inverse photoemission and photoemission if photon energies $> 10\ eV$ are used. There, in principle, all k-vectors in the Brillouin zone may be probed. It is shown in this article that electron states near the Brillouin zone boundary play a key role in band ferromagnets. The photoemission experiment is senior to inverse photo-emission mainly due to the better energy resolution and detection sensitivity of electron– and photon–spectrometers, respectively. Today, an energy resolution of better than 4 meV and a k resolution of better than 0.02 Å^{-1} are obtained with photoemission.

The presented data are recorded with a spectrometer with an overall energy (momentum) resolution of about 50 meV (0.02 $\hbar\text{Å}^{-1}$). This is sufficient for studies at room temperature or above since the thermal broadening of the

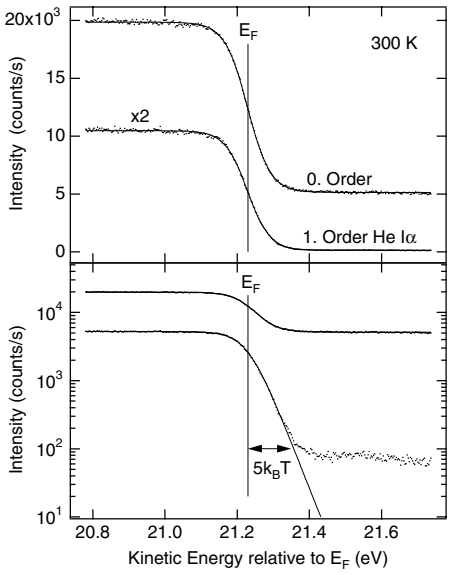

Fig. 2. Photoemission spectra taken around the He Iα Fermi level E_F of polycrystalline silver at 300 K. Unmonochromatized (zero order) and monochromatized (1st order) He Iα radiation was used for excitation. In the lower panel the same data are shown on a logarithmic intensity scale. From Ref.[4].

Fermi function at room temperature corresponds to the convolution of a step function with a Gaussian of 100 meV ($4k_BT$) full width at half maximum. For problems at non zero temperature as it is e.g. the ferromagnetic – paramagnetic phase transition it is possible to probe thermally populated electronic states *above* the Fermi level [4]. Photoemission has thus the potential to measure all relevant states that drive e.g. phase transitions or electron tunneling. This requires a clean and highly intense photon source. Clean means that it should be monochromatic and not have higher photon energy components as e.g. higher harmonics, since these photons produce photoemission above the Fermi level of the main photon energy. The high intensity is needed since the thermal occupation decreases at energies $\Delta\mathcal{E}$ above the Fermi level with $\approx \exp(-\Delta\mathcal{E}/k_BT)$. In our laboratory this setup is realized with a monochromatized ECR plasma driven He gas discharge lamp [4]. In Fig.2 the performance of such a photon source is shown for the photoemission from the Fermi level of a polycrystalline silver sample at 300 K. The logarithmic intensity scale reveals the Boltzmann wing up to $5k_BT$ above the Fermi level. Such measurements of a Fermi level around which the density of states is constant have to be used in order to normalize the photoemission data for a set of energy distribution curves (EDC's) at various emission angles. Then quantitative information on peak positions in energy E and momentum $\mathbf{k}$ can be recovered [1]. For the normalization it is most convenient to subtract a constant background (in the order of $\approx 0.1\%$) of the

average intensity at the Fermi level from the data before normalizing them with the experimentally determined Fermi function. For the purposes of this article an analytical Fermi function of the form $f(E) = 1/(1+\exp(E-E_F/k_BT_{\rm eff}))$ is sufficient. The "effective" temperature $T_{\rm eff} = \sqrt{T^2 + (\Delta {\rm E}/4k_B)^2}$ depends on the sample temperature T and the overall full width at half maximum energy-resolution of the spectrometer ΔE [1]. In the presented experiments the spin polarization is not measured as it is. e.g. done with a Mott polarimeter. This has the drawback of not getting a direct identification of the spin states. On the other hand the sample has not to be macroscopically magnetized over the probed sample area as it is necessary for the measurement of the spin polarization. The assignment of the spin states of direct photoemission transitions is done with help of spin polarized band structure calculations [5]. A further requirement for a band mapping experiment is the accurate control of photoemission direction and an angular resolution below 1°. This is achieved in scanning the sample orientation in front of the detector with an automated high accuracy two angle sample goniometer [4,6,7]. This setup has the advantage of keeping the angle between the photon source and the detector constant and thus avoids matrix element variations that were caused by different light incidences relative to the detector.

3 Angular resolved Photoemission (ARUPS)

There are excellent reviews on photoemission [8], angular resolved photoemission at UV photon energies (ARUPS) in particular [9] and Fermi surface mapping [10]. Photoemission has the potential of measuring all degrees of freedom of an electron in its initial state. It is a local probe since the momentum for the emission is transferred on the photoelectron on a femto second time scale. Nevertheless, it is able to probe the electronic bands of a solid i.e. the delocalized nature of the electron in its initial state. The mapping of the bands is accompanied with a broadening in energy and momentum that has various reasons. Like in lifetime determination from the spectral width in energy, the broadening in k provides a lower limit of extension of the excited states. A band state with an angular width of $0.1{\rm \AA}^{-1}$ has e.g. a spatial extension $\Delta x \geq 10{\rm \AA}$.

3.1 Conservation laws in photoemission

In order to discuss the basic physics (conservation laws) of photoemission it is convenient to use the three step model. There, the photoemission process is described in a sequence of (*i*) the photoexcitation, (*ii*) the transport of the electron to the surface and (*iii*) its refraction at the surface potential barrier and propagation to the detector.

Step (*i*), the photoexcitation, obeys energy–, momentum–, spin– and angular momentum conservation. Energy and momentum conservation are shown in an E vs k diagram in Fig. 3 where a periodic zone scheme for an initial state band and the final state is plotted. If at a given **k**-value, the photon energy matches

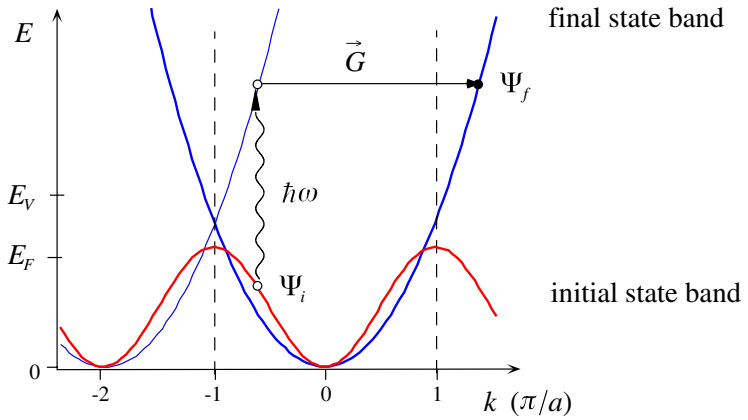

Fig. 3. Photoemission process for band mapping in a periodic crystal in a E vs k scheme. The final state energy, momentum and spin in Ψ_f is related to the initial state Ψ_i via energy, momentum and spin conservation. $\hbar\omega$ is the photon energy and **G** is a reciprocal lattice vector.

the energy difference between an occupied initial state and an unoccupied final state the photoemission is at resonance at this particular point in k-space and a so called direct transition can be observed, if the final state propagates into the vacuum. The photoexcitation is treated as a vertical transition, i.e. the momentum of the photon is neglected: $\omega/c \ll \pi/a$, where a is the lattice constant. This is written down as energy conservation:

$$\mathrm{E}_f = \mathrm{E}_i + \hbar\omega \tag{1}$$

where E_f and E_i are the final and initial state energy and $\hbar\omega$ the photon energy and momentum conservation:

$$\mathbf{k}_f = \mathbf{k}_i + \mathbf{G} \tag{2}$$

where $\hbar\mathbf{k}_f$, $\hbar\mathbf{k}_i$ are the final and initial state momenta and **G** is a reciprocal lattice vector that provides the momentum for propagation to the surface.

It has to be noted that the photoemission process leaves a hole state in the solid i.e. is a $N \rightarrow N-1$ process, where N is the number of electrons in the ground state. Therefore the $N-1$ final state energies E_f do not directly (via Eqn.1) reflect the ground state energy. The interaction of the photoemission hole state with the rest of the solid and the photoelectron is important. This causes a finite lifetime of the final state i.e. a broadening of the observed transitions in energy and momentum. Therefore shifts in energy and momentum with respect to the ground state may occur. For magnetic systems the response on the perturbation upon photo excitation furthermore depends on the spin polarization of the photoelectron and spin dependent correlation effects are important [11]. Transitions from the Fermi level are, however, least affected by these effects since there is only thermal energy available for final state relaxation.

In the photon energy range of interest, the spin orientation of the electrons is conserved:

$$\boldsymbol{\sigma}_f = \boldsymbol{\sigma}_i \tag{3}$$

where $\boldsymbol{\sigma}_f$ and $\boldsymbol{\sigma}_i$ are the spin of the final and initial state.

Finally, the angular momentum character of the photoelectron final state is determined from the dipole selection rules which read in the non relativistic formulation:

$$\ell_f = \ell_i \pm 1; \quad \ell \geq 0 \tag{4}$$

where $\hbar\ell_f$ and $\hbar\ell_i$ are the angular momenta of the final and initial state. For the magnetic quantum number m ($|m| \leq \ell$) we find:

$$m_f = m_i, \tag{5a}$$

$$m_f = m_i \pm 1\,. \tag{5b}$$

where Eqn.5a) applies for linearly polarized light and Eqn.5b) for right– or left circularly polarized light, respectively. The quantisation axis points along the propagation of the photons.

The direction and polarization of the incoming light thus provide selection rules that are useful for the identification of particular bands. The dipole selection rules can be exploited for getting information on the magnetism in performing polarization dependent photoemission experiments. If the sample has a magnetization the photoemission depends on the orientation between the magnetisation and the light propagation and/or polarization (dichroism) [12].

In step (*ii*), the propagation of the photoelectron to the surface, diffraction, elastic and inelastic scattering may occur, but there remains information from the initial state $\Psi_{\rm i}(\mathrm{E_i}, \mathbf{k}_{\rm i}, \boldsymbol{\sigma}_{\rm i})$. In this step differences in the inelastic mean free path between minority and majority spin electrons affect the spectral weight of the observed transitions.

After the last step (*iii*), where the energy for the emission of the photoelectron into the vacuum is payed, the $(N-1)$ photoemission binding energy E_B measured from the Fermi level E_F gets

$$\mathrm{E}_B \equiv \hbar\omega - \mathrm{E}_{kin}^{vac} - \Phi \tag{6}$$

where E_{kin}^{vac} is the electron kinetic energy in the vacuum and Φ is the work function. The surface barrier affects the momentum perpendicular to the surface (refraction). If we make the free electron final state approximation (as it is implicitly done in Fig. 3) we set

$$\mathrm{E}_f \equiv \frac{\hbar^2\mathbf{k}_f^2}{2m_e} \tag{7}$$

and note that m_e is the free electron mass and E_f is measured from the valence band bottom. Then the wave numbers of the initial states $\mathbf{k}_i$ can be determined

from the measured photoelectron momentum $\hbar\mathbf{k}_m$ with the following identities for the components of $\mathbf{k}$ parallel and perpendicular to the surface:

$$\mathbf{k}_{i\|} = \mathbf{k}_{m\|} - (\mathbf{G} - \boldsymbol{n}\mathbf{G}\boldsymbol{n}), \tag{8a}$$

$$\mathrm{k}_{i\perp} = \sqrt{\mathrm{k}_{m\perp}^2 + 2m_e\mathrm{U}/\hbar^2} - \boldsymbol{n}\mathbf{G}. \tag{8b}$$

U is the inner potential, i.e. the energy difference between the vacuum level and the valence band bottom. The surface normal $\boldsymbol{n}$ is parallel to $\boldsymbol{\nabla}U$. If $\boldsymbol{n}$ is constant then $\mathbf{k}_{i\|}$, the component parallel to the surface of $\mathbf{k}_i$ is conserved up to a reciprocal surface lattice vector $\mathbf{Q} = \mathbf{G} - \boldsymbol{n}\mathbf{G}\boldsymbol{n}$. It has to be noted that the conservation of $\mathbf{k}_{\|}$ is given as well without the free final state assumption (Eqn.7). For $\mathbf{k}_{\|}$ conservation the direction of $\boldsymbol{\nabla}U$ has, however, to be constant over the whole sampling area. This follows from $\boldsymbol{n}\mathbf{G} > 0$ and Eqn.8a. For the experiment it is furthermore important to remember that parallel momentum conservation requires zero electric field between the detector and the sample and therefore work function differences between the detector and the sample have to be compensated with a sample bias voltage. If the inner potential varies as it does e.g. for the two spin components in a ferromagnet [13], the determination of the normal component $\mathrm{k}_{i\perp}$ of $\mathbf{k}_i$ is affected. From Eqn.8b and Eqn.2 it is seen that the normal component of $\mathbf{k}_f$ can be measured if $|\mathbf{k}_f| > \sqrt{2m_e\mathrm{U}}/\hbar$ and we call this limit photoemission (PE) horizon (see Fig.4).

Therefore, if E_{kin}^{vac}, $\hbar\mathbf{k}_m$ and σ_f are measured, $\boldsymbol{n}$ and the reciprocal lattice $\mathbf{G}$ are known, the photoemission binding energy E_B, wave numbers $\mathbf{k}_i$, and spin polarization σ_i can be found out by photoemission. If the free final state approximation is not valid, the parallel component of $\mathbf{k}_i$ only is determined. For 20 eV photoelectrons the free final state approximation works astonishingly well while it is expected to become problematic for lower energies. For two dimensional systems, whith no dispersion perpendicular to the surface, the complete information on the electronic states in the Brillouin zone is obtained by a single photon energy. Dispersion perpendicular to the surface can be measured if the photon energy $\hbar\omega$ is scanned as it is conveniently done at synchrotrons.

3.2 k-space mapping

A complete photoemission experiment should sample all points in k-space. If, e.g. the whole second Brillouin zone of nickel down to binding energies of 10 eV shall be scanned, photon energies from 6 eV up to 120 eV have to be at hand and all emission angles should be accessible.

In order to better visualize the angle scanned photoemission experiment it is convenient to redraw Fig. 3. If we sit at a given final state energy E_f, i.e. set the electron analyzer to a fixed kinetic energy E_{kin}^{vac} and use a constant photon energy, the picture in Fig. 3 translates from an E vs. k picture in a $\mathrm{k}_{\|}$ vs. $\mathrm{k}_{\perp}$ picture (see Fig.4). Normally the initial state bands at the chosen binding energy appear as lines. For the final state band the case is particularly simple in the free final state approximation where the final state is a circle centered at the origin

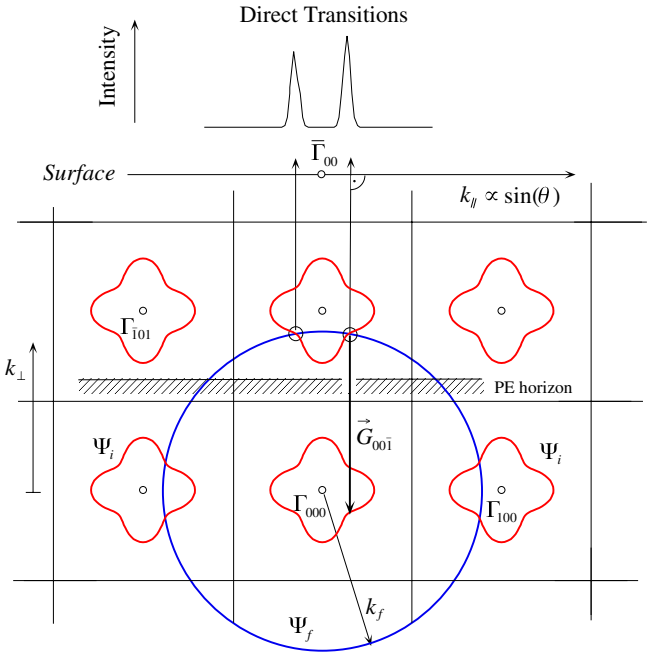

Fig. 4. Photoemission process for band mapping in a $k_{\parallel}$ vs. $k_{\perp}$ picture. Wherever the final state band Ψ_f crosses an initial state band of the periodic zone scheme Ψ_i a direct transition occurs. This transition may be observed above the photoemission (PE) horizon that is a consequence of the surface barrier potential.

of k-space (Γ_{000}) with radius k_f:

$$k_f = \sqrt{2m_e(E_{kin}^{vac} + U)}/\hbar \tag{9a}$$

$$k_f \ [\text{Å}^{-1}] = 0.5123 \sqrt{(E_{kin}^{vac} + U) \ [eV]} \tag{9b}$$

Every intersection point between the initial state band with the periodicity of the reciprocal lattice **G** and the final state indicates a direct transition at the given energy E_B (see Eqn. 6). Parallel momentum conservation projects these states normal to the surface, where they can be measured at the corresponding emission angles:

$$k_{\parallel} = \frac{1}{\hbar}\sqrt{2m_e E_{kin}^{vac}} \ \sin(\theta_m) \tag{10}$$

where θ_m is the measured polar emission angle. The above procedure for k-space mapping is identical to that of Fermi–surface mapping as outlined by Aebi et al. [14]. For Fermi surface maps $E_B \equiv 0$ and correspondingly $E_{kin}^{vac} = \hbar\omega - \Phi$ is the analyzed energy in the detector (see Eqn.6). From Fig.4 it becomes clear that a Fermi surface may be mapped completely, in scanning $\mathbf{k}_f$, i.e. the photon energy and all emission angles, while the analyzer is set to the Fermi energy E_F.

4 Experimental Results

4.1 The Temperature Dependence of the Exchange Splitting in Nickel

Ferromagnetism in metals, i.e. the long range order of electron spins, must be reflected in the Fermi surfaces. They are splitted in a majority (spin up) and a minority (spin down) surface. The exchange interaction that lifts the spin degeneracy of the electronic bands translates in an analogous splitting in **k**-space. Above the Curie temperature ($T_C(Ni) = 627$ K) a ferromagnet becomes paramagnetic and loses the ability to maintain a macroscopic magnetisation. Therefore the **k**-space volume that is enclosed by the two Fermi surfaces must be the same for spin up and spin down electrons. This is e.g. achieved if the exchange splitting of the bands that cross the Fermi level vanishes. It does, however, not mean that any magnetic moment disappears - in nickel the d-shell remains open - but that there is no more long range correlation between the magnetic moments on the lattice sites. Photoemission is able to observe the disappearance of the band splitting as well as local correlation effects above the Curie temperature, as they were e.g. observed with neutron scattering [15] or core level photoemission [16].

Aebi et al. have measured a two dimensional cut across the Fermi surface of Ni(110) below and above T_C [5] and found dramatic changes that can not be ascribed to thermal broadening. Fig. 5 shows this kind of He Iα excited Fermi surface maps from Ni(111) [1]. The photoelectron emission intensity is

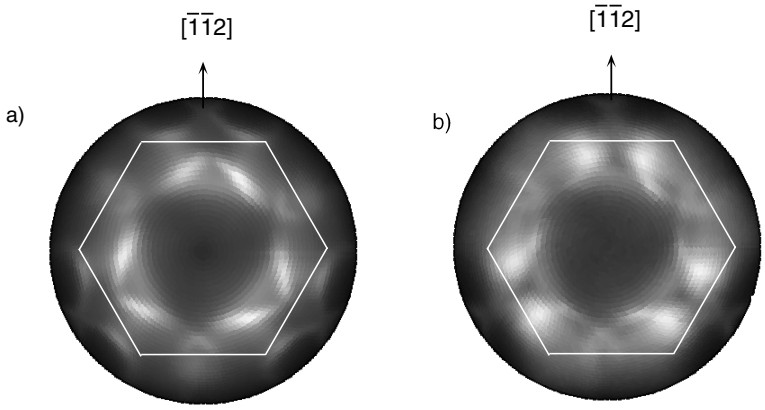

Fig. 5. Fermi surface maps from angular resolved photoemission. The intensity on a linear grey scale (white means high intensity) is displayed as a function of $\sin(\theta)$ and φ, θ being the polar and φ the azimuthal emission angle ($0 \leq k_{\parallel} < 2.06\text{Å}^{-1}$). The hexagons mark the boundary of the first surface Brillouin zone. In a) the He Iα excited Fermi surface map from Nickel (111) at room temperature and b) above the Curie temperature $T/T_C = 1.16$. From Ref. [1].

shown on a linear grey scale where white is the highest intensity. The data are displayed in parallel projection $k_{\|} \propto \sin(\theta)$ (see Eqn.10) with $0 \leq k_{\|} < 2.06 \text{Å}^{-1}$. The azimuthal orientation of the surface and the first surface Brillouin zone are indicated as well. Clearly, the Fermi surface map is three fold symmetric as expected from an *fcc* (111) surface where more than one layer contributes to the photoemission and it becomes evident that dispersion normal to the surface is important. The particular bands of interest were identified by band structure calculations [1]. There are direct minority *d*–band transitions in the first surface Brillouin zone, near the zone boundary, and the ∞–shaped features in the second surface Brillouin zone in the $\bar{1}\bar{1}2$ direction are *sp*–bands and carry minority as well as majority spin electrons (cf. Fig.8a)). It is seen how particular bands move and not simply broaden in k-space if the sample crosses the Curie temperature.

The *sp*–bands that are split in k "collapse" in approaching the Curie temperature. Collapsing means that *sp*–splitting is not observed anymore and that the angular full width at half maximum broadening of the band is less than 0.2 Å^{-1}. The observed collapse of the splitting is in line with a Stoner picture where the exchange splitting decreases with the bulk magnetization. In Fig.6 this collapsing of the *sp*–bands is shown with angular distribution curves (ADC's). The ADC's in Fig.6 show the photoemission intensity at the Fermi level as a function of the azimuthal emission angle ϕ. There the *sp*–bands in the ∞–shaped features at a polar emission angle θ of $78°$ ($k_{\|} = 2.01 \text{Å}^{-1}$) are shown (see Fig. 5). The azimuthal angle $\phi = 0$ refers to the azimuth of the $[\bar{1}\bar{1}2]$ direction. Here an angle step $\Delta\phi$ of $1°$ corresponds to a Δk of 0.035 Å^{-1}. The spin polarization is assigned from comparison with band structure calculations where the inner peaks reflect the minority *sp*– bands while the outer ones those with majority spin [1]. In Fig.6 b) and c) the angular width of the *sp*–band features at the Fermi level are presented as a function of temperature. In Fig.6 b) the data are shown with the thermally induced broadening that increases linearly above T_C. If this linear increase is subtracted below T_C as well, the data fit the bulk magnetization (solid line in Fig.6c)). The data in Fig.6 contain, besides the exchange splitting in k-space, additional information as the width of the individual spin bands and the intensities. This will be further discussed in subsection 4.2..

The *sp*–bands contribute only a few per cent to the magnetic moment of 0.6 μ_B in nickel. The main contribution stems from the hole in the minority *d*–shell. Therefore, the minority *d*–bands at the Fermi level are key players for the magnetism in nickel. In Fig.7 the calculated band structure and measured photoemission cuts across k-space, where the interplay between the *d*–bands and the *sp*–bands is seen, were displayed. The LKKR calculation [18] Fig.7a) shows the expected bands. While the k–locations of the bands are well reproduced, the energies do not correspond to the measurements since renormalization of the energy scale due to self energy and correlation effects ($N \rightarrow N - 1$) are not taken into account in these calculations [11]. A minority *d*–band crosses the Fermi level and appears - in agreement with inverse photoemission [19] - exchange-split by 280 ± 20 meV from its occupied majority sister band. In approaching the Curie temperature the occupied majority band gains energy and merges

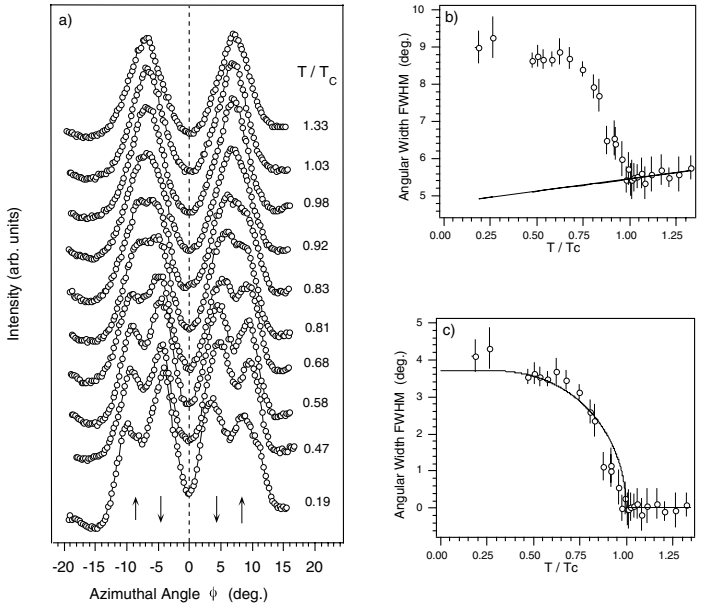

Fig. 6. Temperature dependence of the *sp*–bands. In a) angular electron distribution curves (ADC's) for the emission from the Fermi level taken at various temperatures T/T_C are shown ($T_C = 627\ K$). At lower temperatures the exchange splitting in k-space can be readily observed. In b) the the angular full widths at half maximum of the spin split *sp*–bands are shown. In c) the linear temperature induced broadening is subtracted and it is seen that these data follow the bulk magnetisation (solid line). Data from Ref.[17].

at this particular k–point with the minority band at the Fermi level. In this region of k-space a *sp*–band is very close to the *d*–band. We consider this *sp*-*d* hybrid to be a zone where scattering between $sp_\downarrow$ and $d_\downarrow$ electrons may occur within thermal fluctuations. Such scattering events are a strong perturbation of the local magnetic moment and can thus drive the ferro– paramagnetic phase transition. An analysis of the intensity of the minority and the majority band indeed fuels the proposition [20] that this is a magnetically active region which decreases T_C with respect to the expectations from the Stoner model [21].

4.2 Influence of a Commensurate Insulator on the Magnetism of Nickel

The evolution of the electronic structure of band ferromagnets in interfaces is of key importance for the understanding of phenomena like the giant magneto resistance (GMR) [22] where only recently spin sensitive tunneling junctions became a subject of intense research [23]. It is known that the adsorption of atoms or molecules strongly influences the electronic structure of the surface states of

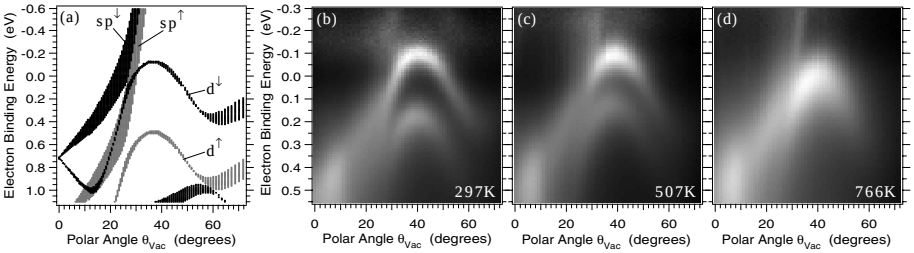

Fig. 7. (a) Spin-polarized LKKR calculation covering the section in **k**-space of the measurements. Majority spin bands are given in gray, minority bands in black. (b)–(d): He Iα excited polar-angle scanned electron distribution curves EDCs taken from Ni(111) along the azimuth which is clock wise 23° off $[\bar{1}\bar{1}2]$, measured at three different temperatures: (b) 0.47 T_C, (c) 0.80 T_C, and (d) 1.21 T_C. From Ref.[20].

nickel [24–28]. Though, the energy and momentum of bulk states were less involved in the interface forming process. There are reports on "intensity shifts" in the bulk bands of nickel upon adsorption of hydrogen [29]. This means that the adsorption of hydrogen on nickel causes strong matrix element effects but no energy or momentum shifts were reported. However, Boschung et al. interpreted these intensity shifts as an indication for the hybridisation of hydrogen with the nickel *d*–band [29].

Here we review the system of one layer of hexagonal boron nitride on Ni(111), where bulk band distortions and intensity redistributions in the *sp*–bands were found [30]. Hexagonal boron nitride forms a perfect commensurate (1x1) overlayer on Ni(111) [31,32]. Nominally *h*–BN is a closed shell sp^2 network within the single layers and is, due to the ionicity of the BN bond, a wide gap insulator ($E_{\mathrm{gap}} = 5.3\ eV$). Therefore it should not contribute with metallic bands to the conduction, nor be magnetic. It is, however, classified to be "metallic" on basis of a soft phonon mode as identified by high resolution electron energy loss spectroscopy (HREELS) [33] and one layer is not thick enough in order to prevent electrons to tunnel across [32]. Fig.8 shows the Fermi surface maps of Ni(111) and *h*–BN/Ni(111). It can be seen that the *h*–BN overlayer with (nominally) no electronic states on the Fermi surface, strongly influences the shape of the Fermi surface of the underlying nickel and therefore the electronic coupling across the interface. The Fermi surface gets distorted and new features emerge. It is seen that the Ni(111) Fermi surface features are replicated three more times in the *h*–BN/Ni(111) case (Fig. 8b)). They are shifted by a primitive reciprocal surface lattice vector **Q**. This is a (1x1) surface umklapp process where the reciprocal lattice vector **G** in the photoemission (see Eqn. 2) contains as well an element of the two dimensional reciprocal surface lattice. The occurrence of such surface umklapps indicates that the *h*–BN layer acts as a grating for any electrons that cross this interface and therefore such umklapps influence the tunneling characteristics of such junctions. Since the *sp*–bands are exchange split (see below) this will affect the spin asymmetry in the tunneling current. From the observation of

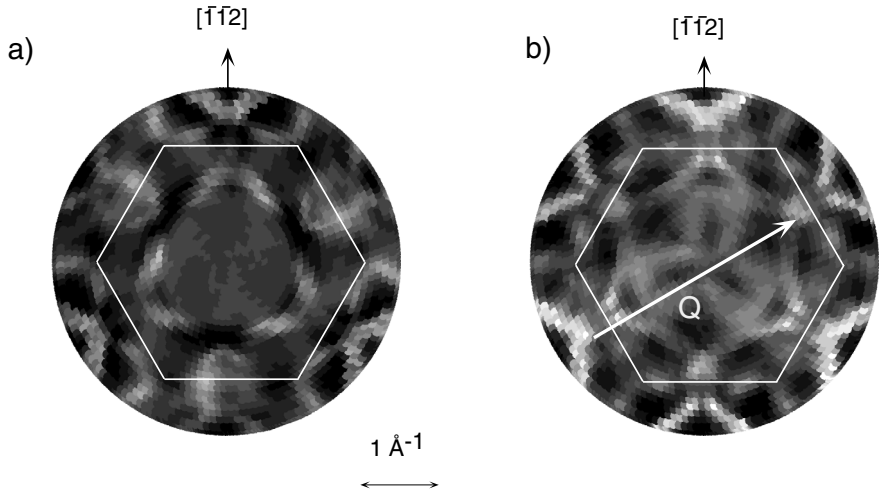

Fig. 8. Fermi surface map from a) Ni(111) measured with He Iβ radiation ($k_{\|} \leq 2.15\text{Å}^{-1}$) and b)$h$–BN/Ni(111)) measured with He Iα radiation ($k_{\|} \leq 2.15\text{Å}^{-1}$) are shown. The differences of a) relative to the Fermi surface maps in Fig.5 are mainly given due to the normalization of the data of each azimuthal scan and much less due to the slightly different photon energy. The hexagons indicate the first surface Brillouin zone. The vector **Q** indicates an umklapp process and is a reciprocal vector of the surface lattice. From Ref.[30].

an umklapp in photoemission it is not straightforward to decide to which extent the initial state is affected since diffraction of the photoelectron in step 2 (transport to the surface) may lead as well to umklapps. An unambiguous indication of an interaction of the overlayer with the substrate are energy and momentum shifts of the electronic states. Intensity variations are more difficult to understand since they involve a quantitative understanding of the matrix element in photoemission.

In Fig. 9 two angular cuts across the *sp*-bands at the Fermi level, in the second surface Brillouin zone of Ni and h–BN/Ni(111), are displayed analogous to the cuts shown in Fig.6. For Ni(111) (h–BN/Ni(111)) the same polar emission angle $\theta_m = 78°$ and the photon energies of 23.1 (21.2) eV were chosen in order to sample the same parallel momenta $\boldsymbol{k}_{i\|}$ at the same emission angles θ_m [34]. The different photon energies compensate for the work function differences of the two surfaces. The four peaks are characterized by their positions, their width and their area A. The k–exchange splitting between the majority and the minority *sp*–band is 0.19 (0.16)Å^{-1}. This decrease of the *sp* exchange splitting in k-space is not expected to be a consequence of the slightly different $k_{i\perp}$ that were probed for the two cases [35]. It is an effect on the initial states at the Fermi energy and

thus indicates the influence of the h-BN on the motion of the electrons in this interface.

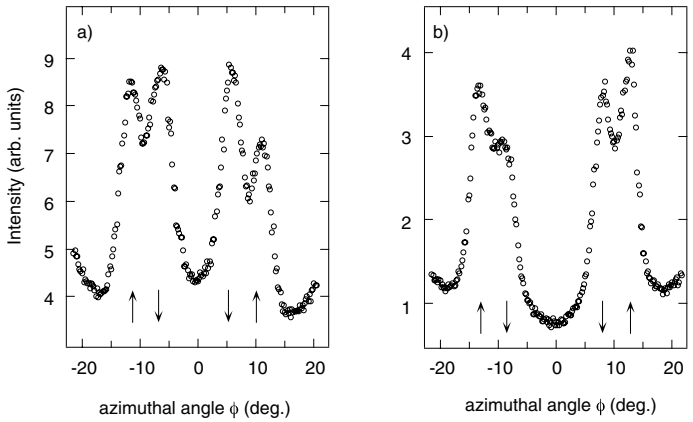

Fig. 9. Photoemission intensity at the Fermi level versus azimuthal angle ϕ. The polar emission angle ($\theta_m = 78°$) is kept constant. φ=0 is defined along the $[\bar{1}\bar{1}2]$ azimuth. The arrows indicate the minority $\downarrow$ and majority $\uparrow$ sp–bands, respectively. a) Ni(111) measured with He Iβ radiation. b)h–BN/Ni(111) measured with He Iα radiation. Note the strong change in the intensity ratio between minority and majority spin transitions. Data from Ref.[30].

The minority sp–band peak width $\gamma_\downarrow$ is about 30% larger than that of the majority bands ($\gamma_\uparrow$). This is in line with a shorter lifetime of minority excitations [36]. In three dimensional systems, however, the connection between the angular broadening and the initial– and final state lifetimes is quite involved [37]. The intensity variation of the spin up / spin down "doublets" left and right from the high symmetry plane are caused by the loss of mirror symmetry due to the oblique incidence of the photons in our experimental setup. It provides a rough estimate for the change of the photoemission matrix element with respect to the orientation of the incoming light. In the following the area ratio $\Upsilon = A_\downarrow : A_\uparrow$ shall be discussed. For Ni(111) ($\Upsilon_{Ni(111)}$=1.7) it does not correspond to that on Ni(100) ($\hbar\omega = 44eV$) found by Petrovykh et al. [38–40] (0.56) nor to that on Ni(110) (0.8) [38,40]. The data from Ref. [41] indicate for Ni(110) and He Iα radiation $\Upsilon_{Ni(110)}$=1.3. Therefore Υ may bank on the experimental parameters and/or the crystal face.

In Fig. 9 an experiment that demonstrates the change of Υ upon the adsorption of a monolayer of hexagonal boron nitride is shown [30]. The change in the area ratio $\Upsilon = A_\downarrow : A_\uparrow = 1.7$ for Ni(111) to 1.1 for h–BN/Ni(111) bears information on the spin dependent electron transmission coefficient. The h–BN overlayer clearly alters the intensities of the spin polarized direct photoemission transitions at these particular places in k-space. This behavior of decreasing Υ upon adsorption of a non-magnetic layer can be related to spin dependent scat-

tering of the electrons during the propagation to the detector (step(*ii*) in the three step model for photoemission). The data in Fig. 9 emphasize that minority photoelectrons get much more efficiently scattered. This is in line with the Siegmann rule [42] stating that at low kinetic energies the inelastic electron scattering cross section is essentially proportional to the number of valence band *d*-holes of a material. Thus for ferromagnets, where the d-holes are polarized, a spin filter effect is expected and in nickel minority spins are scattered more efficiently. In the case of *h*–BN the Siegmann rule predicts no spin filtering since *h*–BN has no polarized *d*–shell. Therefore our finding of a strong asymmetry of the spin transition intensities calls for an extension of the Siegmann rule: it signals that spin filtering may also occur in or due to non–magnetic overlayers that are coupled to a magnetic substrate. This coupling may be mediated by hybridisation of delocalized *sp*–states extending into the interface and/or by the *h*–BN grating on Ni(111) that increases the available phase space for electron hole pair excitations in a spin selective way. Though the umklapps may play a crucial role for the understanding of the magnetic coupling across this interface it has to be emphasized that these very same umklapps may influence the matrix elements of the two spin channels shown in Fig. 9. The possible influence of spin selective hybridisation of the *h*–BN orbitals on the *sp*–bands seems, however, to be unlikely since it is not expected that the *h*–BN bond is selective to the spin of the nickel *sp*–bands. The (essential) assumption of a constant matrix element for a quantitative determination of the spin scattering asymmetry may be hampered by surface umklapp processes [30] and therefore all possible physical mechanisms have to be examined carefully before definite conclusions can be drawn on the absolute value of spin filtering effect of a single layer *h*–BN on Ni(111).

5 Conclusions

Angle scanned photoemission experiments give a detailed insight in the electron dynamics of magnetic interfaces. At the Fermi energy the exchange interaction induced splitting in k-space can be clearly observed and studied as a function of temperature. Within the accuracy of the experiment this splitting is proportional to the bulk magnetisation. For the *h*-BN/Ni(111) interface distortions of the Fermi surface indicate an influence of a nominally non magnetic and non conducting overlayer. The overlayer acts as an atomic grating and produces surface umklapp processes in the photoemission final state. The relative photoemission intensities of spin polarized *sp*-bands are strongly affected by the *h*-BN overlayer. Implications for a new spin–filter effect in h-BN/Ni(111) are discussed.

6 Acknowledgements

It is a big pleasure to acknowledge fruitful collaboration with Thomas Kreutz, Willi Auwärter, Philippe Aebi and Jürg Osterwalder. Felix Baumberger and Matthias Hengsberger critically read the manuscript.

References

1. T.J. Kreutz, T. Greber, P. Aebi, J. Osterwalder, Phys. Rev. B, **58** (1998) 1300.
2. D.T. Pierce and W. E. Spicer, Phys. Rev.Lett., **25** (1970) 581.
3. U. Bänniger, G. Busch, M. Campagna, H.C. Siegmann, Phys. Rev.Lett., **25** (1970) 585.
4. T. Greber, O. Raetzo, T. J. Kreutz, P. Schwaller, W. Deichmann, E. Wetli and J. Osterwalder, Rev. Sci. Instrum., **68** (1997) 4549.
5. P. Aebi, T.J. Kreutz, J. Osterwalder, R. Fasel, P. Schwaller and L. Schlapbach, Phys. Rev. Lett., **76** (1996) 1150.
6. C.S. Fadley, Prog. Surf. Sci., **16** (1984) 275.
7. J. Osterwalder, T. Greber, A. Stuck, L. Schlapbach, Phys. Rev. B , **44**, 13764 (1991).
8. S. Hüfner, Photoelectron Spectroscopy, (Springer, Berlin, 1995)
9. F.J. Himpsel, Advances in Physics, **32** (1983) 1.
10. J. Osterwalder, Surface Rev. and Letters, **4** (1997) 391.
11. F. Manghi, V.Bellini, J. Osterwalder, T. J. Kreutz, P. Aebi and C. Arcangeli Phys. Rev. B, **59** (1999) 10409.
12. G. Van der Laan, Phys. Rev. B, **51** (1995) 240.
13. D. Oberli, R. Burgermeister, S. Riesen, W. Weber and H.C. Siegmann, Phys. Rev. Lett.,**81** (1998) 4228.
14. P. Aebi, J. Osterwalder, R. Fasel, D. Naumović and L. Schlapbach, Surf. Sci., **307-309** (1993) 917.
15. G. Shirane, O. Steinsvoll, Y.J. Uemura and J. Wicksted, J. Appl. Phys.,**55** (1984) 1887.
16. A. Kakizaki, J. Fujii, K. Shimada, A. Kamata, K. Ono, K.-H. Park, T. Kinoshita, T. Ishii, and H. Fukutani, Phys. Rev. Lett., **73** (1994) 2781.
17. T. J. Kreutz, The temperature–dependent electronic structure of nickel metal, (Thesis, Universität Zürich 1997).
18. J.M. MacLaren, S. Crampin, D.D.Vvedensky, R.C. Albers, J.B. Pendry, Comput. Phys. Commun.,**60** (1990) 365.
19. W. von der Linden, M. Donath and V. Dose, Phys. Rev. Lett., **71** (1993) 899.
20. T. Greber, T.J. Kreutz and J. Osterwalder, Phys. Rev. Lett., **79** (1997) 4465.
21. O. Gunnarson, J. Phys. F, **6** (1976) 587.
22. M.N. Baibich, J.M. Broto, A. Fert, F. Nguyen Van Dau, F. Petroff, P. Etienne, G. Creuzet, A. Friedrich and J. Chazelas, Phys. Rev. Lett.,**61** (1988) 2472.
23. J. Maria De Teresa, A. Barthelemy, A. Fert, JP. Contour, F. Montaigne and P. Seneor, Science, **286** (1999) 507.
24. F.J. Himpsel and D.E. Eastman, Phys. Rev. Lett., **41** (1978) 507.
25. M. Donath, F. Passek and V. Dose, Phys. Rev. Lett., **70** (1993) 2802.
26. F. Passek and M. Donath, Phys. Rev. Lett.,**71** (1993) 2122 .
27. H. Namba, N. Nakanishi, T. Yamaguchi and H. Kuroda, Phys. Rev. Lett., **71** (1993) 4027.
28. E. Boschung, Th. Pillo, J. Hayoz, L. Patthey, P. Aebi and L. Schlapbach, J. El. Spectr. and Rel. Phen., **101-103** (1999) 349.
29. E. Boschung, Th. Pillo, J. Hayoz, L. Patthey, P. Aebi and L. Schlapbach, Phys. Rev. B, **58** (1998) R10210.
30. T. Greber, W. Auwärter and J. Osterwalder, In "The Physics of Low Dimensional Systems", Ed. J.L. Morán-López, Plenum, New York, (2001) pg. 411-418.

31. A. Nagashima, N. Tejima, Y. Gamou, T. Kawai and C. Oshima, Phys. Rev. B, **51** (1995) 4606.
32. W. Auwärter, T. J. Kreutz, T. Greber and J. Osterwalder, Surf. Sci., **429** (1999) 229.
33. C. Oshima, A. Itoh, E. Rokuta, T. Tanaka, K. Yamashita, T. Sakurai, Sol. State. Comm., **116** (2000) 37.
34. It is misleading to call this "the same initial state location" as it was done in [30]. Note: if the same initial states ($\mathbf{k}_i$) shall be sampled the same photon energy has to be used, though the polar emission angle depends on the inner potential. In the present case we get from Eqn.9a and Eqn.10 for $k_{f\perp}$ 1.06 and 1.00 Å^{-1} for Ni(111) and h–BN/Ni(111), respectively. The difference corresponds to 2% of the Brillouin zone diameter.
35. In Ni(111) the k-splitting of He Iα excited sp-bands at θ_m=78° is 0.18 Å^{-1}.
36. M. Aeschlimann, M. Bauer, S. Pawlik, W. Weber, R. Burgermeister, D. Oberli and H.-C. Siegmann, Phys. Rev. Lett., **79** (1997) 5158.
37. J.K. Grepstadt, B.J. Slagsvold and I. Bartos, J. Phys. F, **12** (1982) 1679.
38. K.N. Altmann, D.Y. Petrovykh, G.J. Mankey, N. Shannon, N. Gilman, M. Hochstrasser, R.F. Willis and F.J. Himpsel, Phys. Rev. B , **61** (2000) 15661.
39. D.Y. Petrovykh, K.N. Altmann, H. Höchst, M. Laubscher, S. Maat, G.J. Mankey and F. Himpsel, Appl. Phys. Lett., **73** (1998) 3459.
40. F.J. Himpsel, K.N. Altmann, G.J. Mankey, J.E. Ortega and D.Y. Petrovykh, J. of Magnet. and Magnet. Mat., **200** (1999) 456.
41. T.J. Kreutz, P. Aebi, and J. Osterwalder, Sol. State Comm., **96** (1995) 339.
42. H.-C. Siegmann, J. El. Spectr. and Rel. Phen., **68** (1994) 505.